Magnetization measurements of antiferromagnetic domains in $Sr_2Cu_3O_4Cl_2$

Beth Parks
Department of Physics and Astronomy, Colgate University, Hamilton, New York 13346

M. A. Kastner
Department of Physics and Center for Materials Science and Engineering, Massachusetts Institute of Technology, Cambridge, Massachusetts 02139

Y. J. Kim
Center for Materials Science and Engineering, Massachusetts Institute of Technology, Cambridge, Massachusetts 02139

A. B. Harris
Department of Physics, University of Pennsylvania, Philadelphia, Pennsylvania 19104

F. C. Chou
Center for Materials Science and Engineering, Massachusetts Institute of Technology, Cambridge, Massachusetts 02139

O. Entin-Wohlman
School of Physics and Astronomy, Raymond and Beverly Sackler Faculty of Exact Sciences, Tel Aviv University, Tel Aviv 69978, Israel

Amnon Aharony
Department of Physics, Massachusetts Institute of Technology, Cambridge, Massachusetts 02139
and School of Physics and Astronomy, Raymond and Beverly Sackler Faculty of Exact Sciences, Tel Aviv University, Tel Aviv 69978, Israel

(Received 1 November 2000; published 15 March 2001)

The Cu_3O_4 layer in $Sr_2Cu_3O_4Cl_2$ is a variant of the square CuO_2 lattice of the high-temperature superconductors, in which the center of every second plaquette contains an extra Cu^{2+} ion. Whereas the ordering of the spins in the ground-state and the spin-wave excitations of this frustrated spin system are both well understood, we find peculiar behavior resulting from antiferromagnetic domain walls. Pseudodipolar coupling between the two sets of Cu^{2+} ions results in a ferromagnetic moment, the direction of which reflects the direction of the antiferromagnetic staggered moment, allowing us to probe the antiferromagnetic domain structure. After an excursion to the high fields (>1 T), as the field is lowered, we observe the growth of domains with ferromagnetic moment perpendicular to the field. This gives rise to a finite domain wall susceptibility at small fields, which diverges near 100 K, indicating a phase transition. We also find that the shape of the sample influences the domain-wall behavior.

DOI: 10.1103/PhysRevB.63.134433 PACS number(s): 05.70.Fh, 75.25.+z, 75.30.Cr, 75.60.−d

I. INTRODUCTION

Domains in antiferromagnets are not frequently studied because they are very difficult to observe. While domain walls in ferromagnets are marked by a change in the uniform magnetic moment at the wall, domain walls in antiferromagnets have no such marker. Domains can be sometimes studied through their effect on the width of magnetic neutron-scattering peaks; however, this broadening is measurable only if the domains are quite small. For materials with larger domains there are generally no experimental methods to observe the motion of the walls.

In this paper, we describe investigations of antiferromagnetic domain walls in $Sr_2Cu_3O_4Cl_2$. This system is unusual in that a small ferromagnetic moment reflects the local antiferromagnetic order, allowing us to infer the behavior of the antiferromagnetic domains from the uniform magnetization. The uniform magnetization at low fields is the result of the presence in $Sr_2Cu_3O_4Cl_2$ and $Ba_2Cu_3O_4Cl_2$ (''2342'') of a novel variant of the CuO_2 layer found in the high-temperature superconductors. The structure of this material is shown in Fig. 1. It consists of Cu_3O_4 planes separated by spacer layers of SrCl. Every second plaquette of the CuO_2 lattice contains an additional Cu^{2+} ion in its center, creating two interpenetrating square lattices of Cu ions.[1,2] The Cu ions forming the conventional CuO_2 layer (labeled Cu_I) have a very large Cu_I-Cu_I antiferromagnetic coupling ($J_I = 130$ meV), similar to that in the high-T_c parent compounds. Because of the weak interplanar coupling, this results in three-dimensional antiferromagnetic order at a Néel temperature T_I near 380 K.

Unlike in the CuO_2 layers of some high-T_c compounds, the structure is perfectly tetragonal. Therefore, the Cu d^9 ions at the center of the squares (labeled Cu_{II}) are surrounded by four equidistant Cu_I neighbors and the isotropic Heisenberg interaction between Cu_I and Cu_{II} spins is frustrated; thus, the two Cu sublattices are almost decoupled. The weaker Cu_{II}-Cu_{II} coupling then gives antiferromagnetic

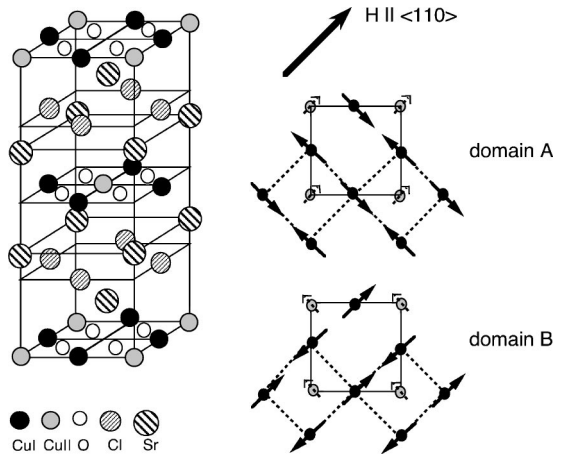

FIG. 1. Structure of $Sr_2Cu_3O_4Cl_2$ (left) and of the Cu_3O_4 layer (right), including two domain configurations for $\mathbf{H}\|\langle 110\rangle$. In domain *A* the moments of the Cu_{II} spins, shown as small arrows on the open circles, are parallel to the applied magnetic field, resulting in a longitudinal moment. In domain *B* the moments of the Cu_{II} spins are perpendicular to the applied magnetic field, resulting in a transverse moment. The figure shows only the part of the moment induced by the internal pseudodipolar field. There also exists an additional small canting of the Cu_I moments.

order at a separate lower Néel temperature $T_{II} \approx 40$ K.[3–6]

One prominent feature of this system is a small permanent ferromagnetic ($H \to 0$) moment that appears at the Néel temperature of the Cu_I ions. Chou *et al.*[7] have shown that the permanent moment arises from the pseudodipolar interaction between the spins of the Cu_I ions and those of the Cu_{II} ions. This results from the bond dependent anisotropic Cu_I-Cu_{II} superexchange coupling.[7] One would expect this ferromagnetic moment to align with an applied magnetic field, such as in the configuration labeled domain *A* in Fig. 1. Thus, the external uniform field generates an effective *staggered field* on the Cu_I spins, allowing us to probe the effects of such a field on the antiferromagnetic domains. The observation of domains with the second configuration, labeled domain *B*, will be the subject of much of this paper.

Recently, Kastner *et al.*[8] used measurements of the magnetization at fields from a few hundred gauss to 5 T to determine a number of terms in the spin Hamiltonian. Neutron-scattering studies of the spin-wave spectrum by Kim *et al.*[9] determined other terms and, most importantly, showed how quantum fluctuations result in the ordering of the Cu_{II} sublattice staggered magnetization parallel to that of the Cu_I staggered magnetization at low temperature. Thus, the Hamiltonian that describes this interesting system appears to be very well established: both the Cu_I and Cu_{II} subsystems are well described by the two-dimensional square lattice Heisenberg model, with the largest correction terms (related to the out-of-plane anisotropy, which forces the spins into the *XY* plane) of relative order 10^{-2}. The in-plane anisotropies are much smaller, of relative order 10^{-7}. Antiferromagnetic domain walls in such a system are expected to be very wide and have very low creation energy. That is, the mass of the solitons is expected to be very small. Since the creation of walls gains entropy, such systems are good candidates for the spontaneous creation of walls.

Given our understanding of the spin Hamiltonian, the behavior we report here of the magnetization at fields below a few hundred gauss seems surprising. We find that when the field is reduced from a high value, the moment parallel to the field decreases and a moment develops perpendicular to the field. That is, the system develops domains with the ferromagnetic moment rotated by $\pi/2$ relative to the field direction. This second type of domain is labeled ''domain *B*'' in Fig. 1. Furthermore, these domains undergo a phase transition at ~ 100 K, resulting in a divergent domain-wall susceptibility. Our aim in this paper is to describe the phenomenology of the domain-wall behavior in order to stimulate further work to elucidate the underlying physics.

In Sec. II we present experimental details. In Sec. III we present measurements of magnetization as a function of temperature and field. We have determined the moment both parallel and perpendicular to the field for samples that are rectangular in shape as well as square. Section IV is devoted to a discussion of the results. There we discuss the phase transition in the domain-wall system.

II. EXPERIMENTAL DETAILS

We have focused on the material $Sr_2Cu_3O_4Cl_2$, since we have grown large single crystals of it by slow cooling from the melt. For the magnetization measurements, we cut from these crystals small square cross-section samples, with dimensions up to $6 \times 6 \times 0.5$ mm having the *c* axis (normal to the Cu_3O_4 layer) perpendicular to the large face and long edges parallel to the $\langle 110\rangle$ axes. The rectangular samples used to study the shape dependence have dimensions approximately 2×7 mm parallel to the $\langle 110\rangle$ axes and have thicknesses of approximately 0.5 mm parallel to the *c* axis. The latter crystals are oriented with either the 7 mm edge (called the ''long side'') or the 2 mm edge (called the ''short side'') parallel to the applied field.

We have also made measurements on smaller single crystals of $Ba_2Cu_3O_4Cl_2$, as well as polycrystalline samples. Measurements of the magnetic moment as a function of magnetic field and temperature are made with a Quantum Design SQUID magnetometer at fields up to 5 T. Our magnetometer is equipped with a special coil allowing measurement of the moment transverse to the field (M_t), as well as parallel to the field. We use *M* to indicate the longitudinal moment, measured parallel to the field, throughout this paper.

In order to reveal the interesting domain phenomena at low fields most clearly, it is important to begin at the high fields and then decrease the field to less than 100 Oe. Unfortunately, when this procedure is followed, the superconducting magnet in our magnetometer traps some flux, resulting in a small residual field at zero magnet current. To characterize this, we have measured the moment as a function of the field for a platinum standard. We find that after an excursion to 2 T, the moment varies linearly with the field but with a residual field at zero current of approximately -5.0 Oe. The residual field is opposite to the direction of the field during the high-field excursion, so that after the field is reduced from a high positive value, the field inside the

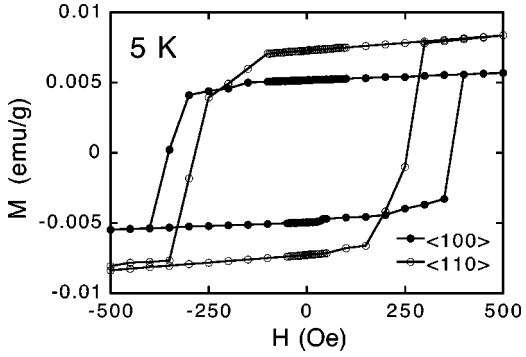

FIG. 2. $M(H)$ at 5 K for fields along the $\langle 110\rangle$ and $\langle 100\rangle$ crystal axes. The moment is $\sqrt{2}$ larger and the coercive field is $\sqrt{2}$ smaller for $\langle 110\rangle$.

magnet will actually be zero when the nominal field obtained from a measurement of the magnet current is $+5$ Oe. Throughout this paper, our figures show the nominal value of H as determined from the current through the magnet without making the correction for the trapped flux.

III. RESULTS

Chou *et al.*[7] and Kastner *et al.*[8] have published measurements of M as a function of field for H greater than a few hundred oersted. They find that the extrapolation of the moment to the zero field gives a permanent moment along a $\langle 110\rangle$ direction. We call this the saturated moment M_s. At lower fields, one sees hysteresis as expected for a ferromagnet. In Fig. 2, $M(H)$ is plotted for $H\|\langle 110\rangle$ and $H\|\langle 100\rangle$ at $T=5$ K. This temperature is below T_{II}, so that both Cu_I and Cu_{II} spins are ordered. These hysteresis loops illustrate that $\langle 110\rangle$ is the easy axis, since for the $\langle 100\rangle$ direction the moment is smaller by $\sqrt{2}$ and the coercive field is larger by $\sqrt{2}$. This is consistent with the interpretation of Kastner *et al.* that the Cu_{II} moments are collinear with those of the Cu_I's at low temperatures, as required by the quantum fluctuations of the Cu_I-Cu_{II} interactions.[9,10]

As T is increased toward T_{II}, the coercive field decreases dramatically, from ~ 300 Oe, as seen in Fig. 2, to ~ 50 Oe at T_{II}. For the remainder of this paper, we discuss the unusual behavior of the hysteresis along the easy axis $\langle 110\rangle$ above T_{II}. To obtain an overview of the behavior, first consider the hysteresis loop at high temperature 200 K shown in Fig. 3. One can see that the extrapolation of the moment from high field to $H=0$ gives $M_s \sim 0.007$ emu/g, the value found by Chou *et al*. However, deviations from $M=\chi_{110}H+M_s$ are clear below about 500 Oe. As mentioned above, the coercive field H_{coer} is identified by the sudden jump in M, and is much smaller than at 5 K.

Figure 4 shows hysteresis loops at 120 K for the longitudinal and transverse moments. It is important to emphasize that although the magnetic moment is measured only for small fields, the field is swept up to at least 1 T in each direction before reducing the field toward zero. The effect of a smaller field range on the hysteresis loop will be discussed later. Unless otherwise stated, all loops are measured with high-field excursions.

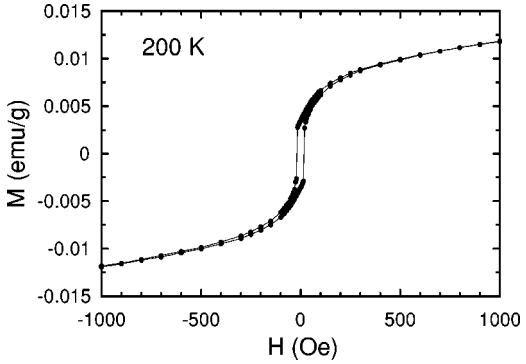

FIG. 3. $M(H)$ at 200 K. This measurement is made with the field parallel to the long side of the rectangular sample. Note that the coercive field is much smaller than at lower T (Fig. 2) and that the moment deviates from its linear dependence on H for fields below ~ 500 Oe. In this plot and in all subsequent plots $H\|\langle 110\rangle$.

First focus on the longitudinal moment in Fig. 4(a). As for the data at 200 K, the magnetic moment parallel to the field decreases below its saturated value before the field reaches zero, although at this temperature the deviation is only seen at much lower fields than at 200 K. Furthermore, upon passing through zero field, the moment decreases further and appears to approach zero as the field is made more negative, before suddenly jumping to a large negative value at

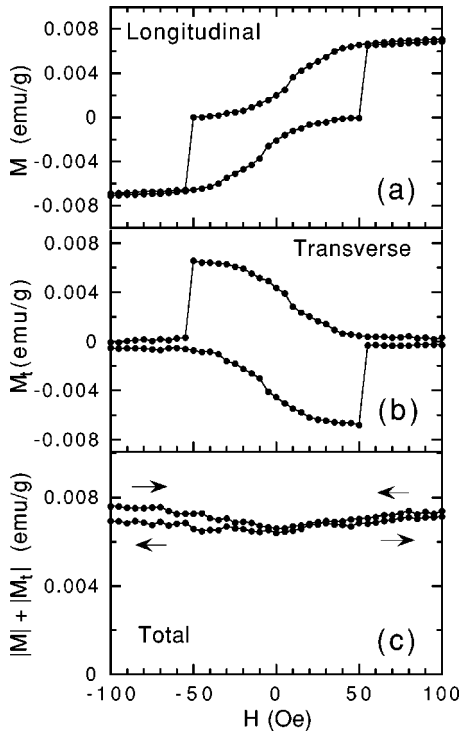

FIG. 4. (a) Longitudinal, (b) transverse, and (c) the sum of the absolute values of the moments versus H at 120 K. Although measurements are shown only for small fields, the field is swept between $+5$ and -5 T. Only after excursion to high fields are loops like those in (a) and (b) observed. These measurements are made with a rectangular sample, and the magnetic field is parallel to the long side.

$-H_{coer}$. The inflection point on the curve for the decreasing field appears to occur at a small positive field. (The inflection points will be labeled H_{inf} in the rest of this paper.) For this hysteresis curve, H_{inf} is consistent with the zero field; the offset results from the flux pinning as discussed above.

Figure 4(b) illustrates that the decrease in the longitudinal moment results from a change in the direction of the sample's ferromagnetic moment from parallel to perpendicular to the magnetic field. In Fig. 4(b) we plot the transverse moment measured for the same sample as for Fig. 4(a). One sees that the decrease in the longitudinal moment is compensated by an increase in the transverse moment. The sign of the transverse moment is arbitrary; we sometimes see one sign and sometimes the other. We assume that a small misalignment between the field and the crystal axes determines the sign. In this experiment, the transverse moment is close to zero at ± 100 Oe. However, we sometimes see a small residual transverse moment, which we also ascribe to a slight misalignment of the sample axes relative to the field.

Figure 4(c) shows that $|M|+|M_t| \simeq M_s$, independent of the field. This demonstrates that after the sample is prepared by an excursion to the high field, at the low field it contains some domains polarized parallel to the field and other domains polarized in one of the two directions perpendicular to the field. Were the moment, instead, rotating continuously with the field, the longitudinal and transverse components would add in quadrature to give M_s. The latter possibility is also prohibited by the anisotropy energy determined previously.[7,8] Furthermore, were a significant volume fraction of the domains in the sample magnetized in opposite transverse directions, then the sum $|M|+|M_t|$ would be reduced. We emphasize that this behavior is only observed if the field is swept over a wide field range, say 1 to -1 T and back again. If the sweep range is smaller, the behavior is different, as discussed below.

Figure 4 indicates that transverse domains grow in size as H is decreased. This begins even for $H>0$ where the transverse domains cost energy $M_s H$ per unit volume. Therefore, there must be a reduction in the free energy when domains are created with moments rotated relative to each other by $\pi/2$. We suggest that this gain in free energy may come from the entropy of the additional domain walls, as discussed below. Note that the stabilization of domains in this system cannot result from dipolar effects as in conventional ferromagnets. First, such dipolar effects would reduce the magnitude of the moment of the sample, not simply exchange a transverse moment for a longitudinal one. Second, the magnetization of our crystal is so small that the dipolar effects would overcome the external field only at much smaller fields ~ 0.3 Oe. Therefore, the effect must come from the antiferromagnetic interactions.

In Fig. 5, we sketch our understanding of the domain structure at several points on the hysteresis loop. The figure is not intended to show the exact shape, size, or number of domains, since we cannot determine that from our experiments.

The qualitative shape of the hysteresis loop is the same from ~ 150 K down to ~ 60 K, but the susceptibility $\chi = dM/dH$ at H_{inf} becomes larger as one lowers the temperature toward 100 K and then becomes smaller again below 100 K. We have subtracted the high-field susceptibility, which is primarily due to canting of the Cu_I ions, to determine the contribution to the susceptibility from domains and plot its inverse χ^{-1} at H_{inf} in Fig. 6. This shows the divergence of the domain-wall susceptibility suggesting a phase transition near 100 K.

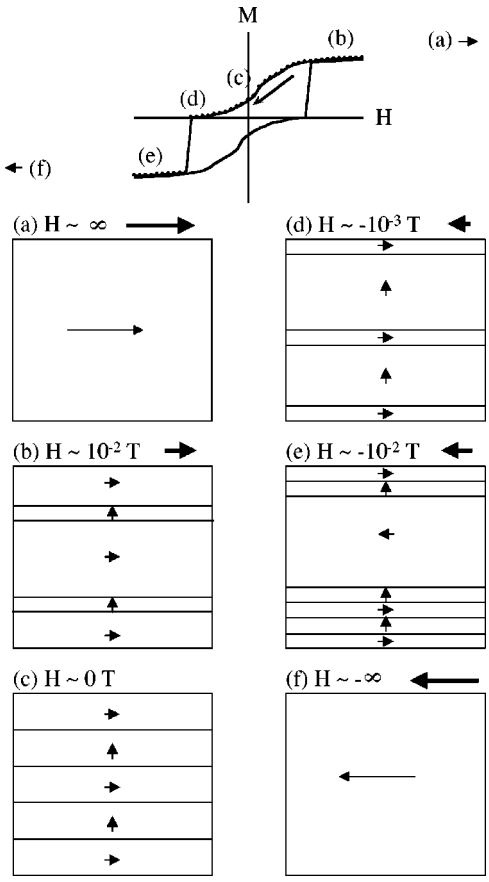

FIG. 5. A sketch of the domains at some points in a hysteresis loop. Arrows in the domains indicate the direction of the ferromagnetic moment. Domain shapes are arbitrary. (a) Starting at the high field, the sample is either single domain (as shown) or has transverse domains of negligible volume. (b) As the field is decreased, transverse domains are formed that decrease the longitudinal moment. (c) At zero field, equal volumes of the sample are occupied by two perpendicular domains. (d) When the field direction is reversed, the transverse domains, which are favored by the energy HM_s, grow to fill nearly the entire sample. (e) A new domain is nucleated parallel to the field at $-H_{coer}$. This domain grows quickly to fill the sample, but the other domains are not destroyed. The evidence for this conclusion is discussed in conjunction with Fig. 10. (f) At some negative field, the unfavored domains are destroyed. We are unable to determine whether this field is reached in our experiments.

Figure 7 illustrates the phase transition in another way. In this experiment, a field of 5 T is applied while cooling the sample to 5 K, after which M and M_t are measured in a 10 Oe field while increasing the temperature. As T increases, M retains its saturation value up to T_{II}, and then suddenly decreases. As T approaches the phase transition at

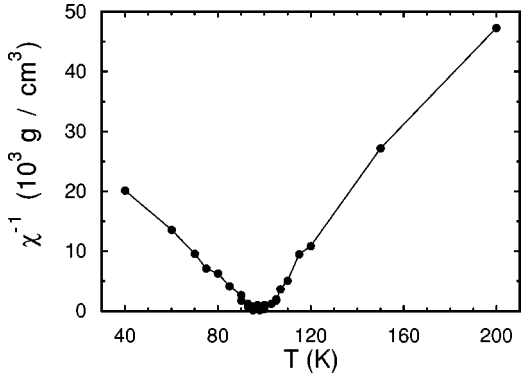

FIG. 6. From hysteresis loops like that in Fig. 4(a), we find $\chi = dM/dH$ at the inflection point H_{inf} and subtract the high-field susceptibility, leaving the component resulting from domain-wall motion. χ^{-1} is plotted versus T for a square sample.

100 K, the moment increases up to the saturation value, and then decreases above the transition because only near the transition is this small field sufficient to saturate the moment. The transverse moment shows the complementary behavior. We have multiplied each set of data by a factor close to one to allow for possible misalignment of the crystal. When these scaled data are added together, the sum of the magnitudes of the longitudinal and transverse moments is in good agreement with the saturated moment reported by Chou *et al.*,[7] determined by extrapolating $M(H)$ from high field to $H = 0$.

Figure 8 shows neutron-scattering data that confirm that the change in the magnetic moment near 100 K is due to a change in the relative size of the domains. These data show the intensity of the (321) magnetic Bragg peak as a function of temperature in nominally zero magnetic field. Neutron scattering is sensitive only to the spin component perpendicular to the momentum transfer. As a consequence, the ratio of scattered intensity for one domain in Fig. 1 to that of the other for the (321) Bragg reflection is only 0.05. As the temperature passes through 100 K, we see that the magnitude

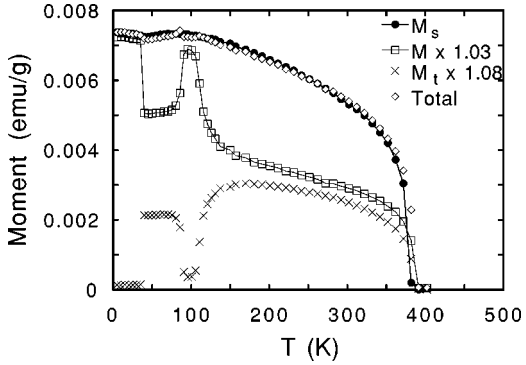

FIG. 7. Moment measured while warming the sample at 10 Oe after cooling in 5 T. The longitudinal and transverse moments have each been multiplied by a correction factor to allow for possible sample misalignment. The moment M_s is measured by extrapolating the linear $M(H)$ at high field (see Fig. 2 for example) down to $H = 0$. Only small percentage corrections are needed to make the sum of longitudinal and transverse moments agree with M_s.

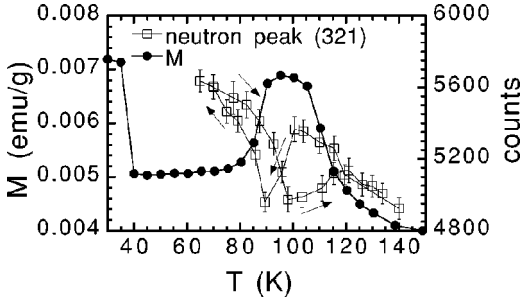

FIG. 8. Neutron-scattering (321) peak intensity as a function of temperature in nominally zero magnetic field. The data for $M(T)$ from Fig. 7 are also plotted for comparison. As the temperature passes through 100 K, we see that the neutron peak intensity decreases, implying that the domain that has stronger magnetic Bragg scattering peak at this location is shrinking while the domain with weaker scattering is growing. This change in peak intensity is riding on a large background because (321) is also the location of an allowed nuclear Bragg reflection.

of the peak decreases, implying that the weakly scattering domain is growing in size. This change in peak intensity is riding on a large background, since (321) is also the location of an allowed nuclear Bragg reflection. We notice that there is hysteresis in the temperature dependence of the peak intensity. Some hysteresis is also observed in the measurement of M when temperature is swept up and down through 100 K.

In Fig. 9 we plot the hysteresis loop at 100 K. At this temperature, close to the phase transition, the longitudinal moment remains at its saturation value all the way down from a high-positive field to $H = 0$ and then suddenly becomes completely transverse as soon as the field is made slightly negative. (The field from trapped flux appears to be closer to 10 Oe than 5 Oe in this case.) This is consistent with the divergent susceptibility discussed above. Despite the striking change in susceptibility, the moment at H_{inf} is close to $M_s/2$ for all temperatures from 40 to 300 K. This will be important for our discussion below.

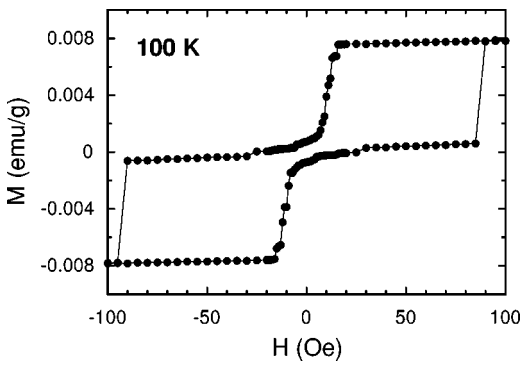

FIG. 9. Hysteresis loop with excursions to ± 5 T at 100 K for field along the short side of the rectangular sample. (The results for the field along the long side are similar.) At this temperature, the moment becomes completely transverse as soon as the field is reduced to zero. Note that flux trapping shifts the zero field point to ~ 10 Oe after an excursion to 5 T and ~ -10 Oe after an excursion to -5 T.

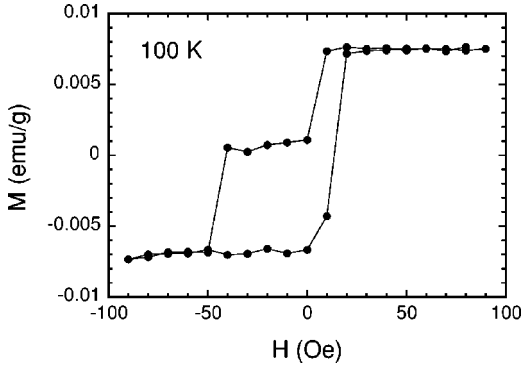

FIG. 10. Asymmetric hysteresis loop at 100 K. Beginning at +1 T, the field is swept to −90 Oe, then to +90 Oe. The asymmetry implies that some domains with positive moment persist even when most of the sample has negative moment.

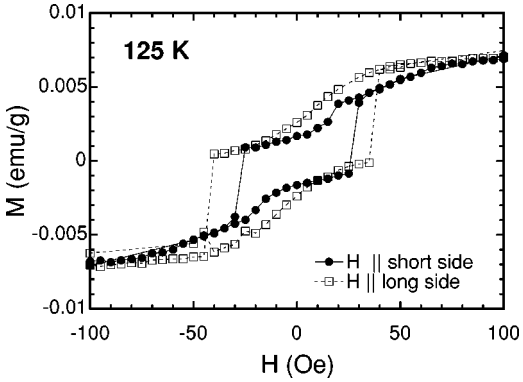

FIG. 11. Hysteresis loops for fields parallel to the long and short sides of the rectangular sample. The data for the long side have been scaled by a factor 1.09 to make the moments agree at 100 Oe. We assume that the correction factor is necessary because of sample misalignment.

The transverse domains are metastable at a large enough negative field. The sudden jump to the negative longitudinal moment that occurs at $-H_{coer}\sim-100$ Oe at 100 K (Fig. 9) signals the nucleation of domains with the moment parallel to the applied field. However, we find that some of the domains with the moment antiparallel to the field survive, and that different domains are destroyed at different fields. We show this in Fig. 10. This experiment begins with the field at 1 T; we then reduce the field to zero and perform small hysteresis loops of increasing size. For the smallest loops (out to $|H|<70$ Oe) $M=M_s$ at positive fields and $M=0$ at negative fields. For a loop that extends to ± 80 Oe, the longitudinal magnetization changes from zero to $-M_s$ at -80 G, but returns directly to $+M_s$ at positive fields without developing a transverse moment. The next hysteresis loop, which extends to ± 90 Oe, is shown in Fig. 10. Even though domains with magnetization $-M_s$ were formed in the previous hysteresis loop, they were evidently destroyed by the excursion to $+90$ Oe, since, when the field is decreased through zero in this hysteresis loop, no domains with magnetization $-M_s$ are formed until the field reaches -50 Oe. We infer that domains with the positive moment formed at +1 T are not all destroyed at small negative fields (although the domain walls must be pushed very close together), but that domains with the negative moment formed at -80 Oe are all destroyed at $+90$ Oe. Also, in the sections of these loops in which the magnetization changes directly from $+M_s$ to $-M_s$ we still observe some hysteresis of order 10 Oe. This tells us that the effects of pinning are generally small, but perhaps not negligible.

We have found that sample shape has a small but significant effect on the hysteresis loops. In Fig. 11, $M(H)$ is plotted at $T=125$ K for the two orientations of the rectangular (2×7 mm) sample. It is apparent that H_{inf} is different for the two orientations. As illustrated in Fig. 12, when the field is applied parallel to the short side of the rectangular sample H_{inf} increases linearly with temperature. However, when H is parallel to the long side, there is little if any variation of H_{inf} with temperature, and the inflection field is consistent with zero field, taking into account the 5 Oe offset from trapped flux. Thus, the inflection point occurs at higher fields for the short side than for the long side above 100 K, but the opposite is true below 100 K. At temperatures above 140 K it is difficult to identify an inflection point because the susceptibility is constant over a wide range of applied magnetic fields. The behavior of H_{inf} for a square sample is intermediate between that for the long and short sides of the rectangular one.

We emphasize that this shape effect cannot result from different demagnetization effects for the different orientations. The maximum magnetizations are of order 10^{-2} emu/g. This results in a maximum demagnetization field of order 0.3 Oe, which is much smaller than the observed shifts in H_{inf} of up to 20 Oe.

Although H_{inf} is affected by the sample shape, H_{coer}

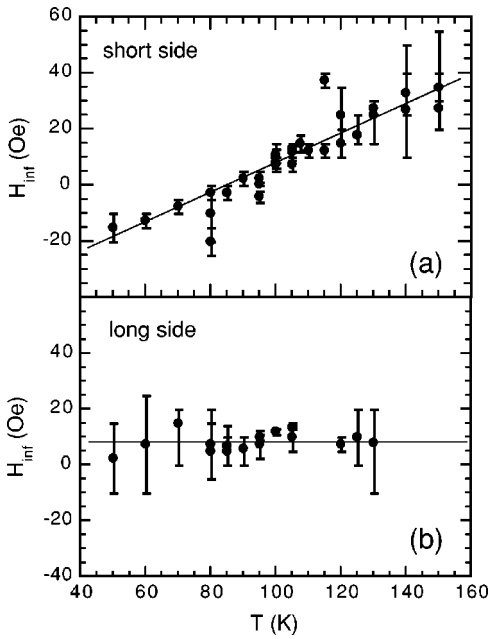

FIG. 12. From data like those in Fig. 11, we determine the inflection point H_{inf} at each temperature. These are plotted for the H parallel to the short side in (a) and the long side in (b).

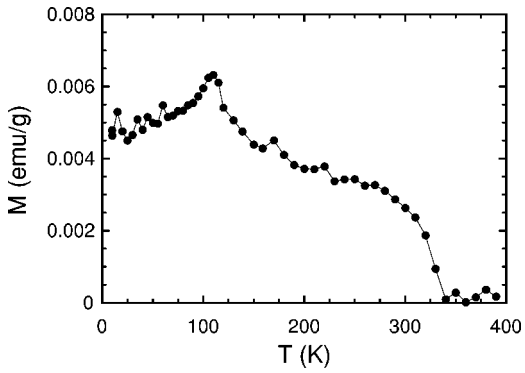

FIG. 13. The moment for a small single crystal of $Ba_2Cu_3O_4Cl_2$ as a function of temperature. The moment was measured on warming in 5 Oe after cooling in the same field.

shows no systematic variation. The latter varies between different hysteresis loops for the same sample at the same temperature as much as it does between different sample shapes.

Our last result, shown in Fig. 13, is $M(T)$ measured in a 5 Oe field for $Ba_2Cu_3O_4Cl_2$. We have not studied this material in the same detail as the Sr compound because much larger crystals are available for the latter. Nevertheless, it is clear that the domain walls show the same behavior. Indeed, the phase transition occurs at almost the same temperature, despite considerable differences in a *c*-axis lattice constant and melting point. We have also observed qualitatively similar magnetization curves for sintered polycrystalline samples of both materials.

IV. DISCUSSION

As discussed by Chou *et al.*,[7] following the theory of Yildirim *et al.*,[11] the most general form of the interaction between a Cu_I and a neighboring Cu_{II} is

$$\mathcal{H}_{\text{I-II}} = J^{\parallel} S_I^{\parallel} S_{II}^{\parallel} + J^{\perp} S_I^{\perp} S_{II}^{\perp} + J^z S_I^z S_{II}^z, \tag{1}$$

where $\parallel$ and $\perp$ denote parallel and perpendicular to the Cu_I-Cu_{II} bond. This form follows from general symmetry arguments, and is also derived perturbatively from the five-band Hubbard model. Summing over the four Cu_I-Cu_{II} bonds yields the interaction

$$\mathcal{H} = \mathbf{M}_{II} \cdot (J_{\text{av}} \mathbf{M}_I + J_{\text{pd}} \hat{\Gamma} \mathbf{M}_I^{\dagger}) \tag{2}$$

per Cu_{II} spin, where $\mathbf{M}_I$ and $\mathbf{M}_I^{\dagger}$ denote the local uniform (ferromagnetic) and staggered moments of the Cu_I sublattice, respectively, and $\mathbf{M}_{II}$ is the uniform moment of the Cu_{II} sublattice. Here,

$$J_{\text{av}} = \tfrac{1}{2}(J^{\parallel} + J^{\perp}), \quad J_{\text{pd}} = \tfrac{1}{2}(J^{\parallel} - J^{\perp}), \tag{3}$$

and $\hat{\Gamma} \equiv \sigma_z$ is the 2×2 Pauli matrix that rotates (x,y) into $(x,-y)$, that is, $\hat{\Gamma}(x,y) \equiv (x,-y)$. It is clear from Eq. (2) that, in addition to the isotropic average exchange J_{av}, the term involving J_{pd} represents an *anisotropic* net interaction. It has the same symmetry as the dipolar field at the center of the plaquette due to four magnetic point dipoles at the Cu_I sites; it is therefore called the pseudodipolar interaction. This term represents a bilinear coupling between $\mathbf{M}_I^{\dagger}$ and $\mathbf{M}_{II}$. Therefore, when $\mathbf{M}_I^{\dagger}$ orders below T_I, it generates a net field $-4J_{\text{pd}}\hat{\Gamma}\mathbf{M}_I^{\dagger}$ on the Cu_{II} in the center of each plaquette. Since the Cu_{II}'s occupy only every second plaquette (both in each plane and in neighboring planes), they are all surrounded by exactly the same configuration of Cu_I moments in each plane, and therefore, have the same ferromagnetic moment. The pseudodipolar coupling J_{pd}, which connects the ferromagnetic moment with the antiferromagnetic moment on Cu_I, enables the study of *antiferromagnetic* domains in $Sr_2Cu_3O_4Cl_2$.

As Yildirim *et al.*[11] explain, the quantum fluctuations involving the anisotropic Cu_I-Cu_I interactions generate an effective fourfold anisotropy of the form $\mathcal{H}_4 = -K\cos(4\theta)$, where θ is the angle between the staggered moment and the Cu_I-Cu_I bond. This anisotropy prefers ordering along these bonds. For this ordering, Eq. (2) then implies that the uniform moment on the Cu_{II} ions points in a direction rotated by $-\pi/2$ relative to the staggered moment on the Cu_I ions. This ordering is also favored by the small ferromagnetic moment $\mathbf{M}_I$, which prefers to be orthogonal to $\mathbf{M}_I^{\dagger}$. Examples are shown in Fig. 1. In discussing our results, it is important to remember that at zero external field the four possible directions of the ferromagnetic moment correspond to the four possible directions of the staggered moment on the Cu_I's. Thus, applying a large enough magnetic field along a $\langle 110 \rangle$ direction creates a single antiferromagnetic domain, of the type *A* in Fig. 1, throughout the sample.

Upon reducing the field from a high value at any temperature in the range $T_I > T > T_{II}$, we observe the growth of domains with the moment perpendicular to the field. This requires the presence in the sample of $\pi/2$ domain walls and a pressure on the walls tending to cause the transverse domains to expand in volume against the pressure HM_s favoring longitudinal domains. (See Figure 5.) The growth of transverse domains continues when the field is reversed until the negative field reaches $-H_{coer}$, at which new $\pi/2$ domain walls are created (within the transverse domains) to form domains with moments parallel to the reversed field.

It is useful to compare the behavior of the domains in this system with those in a conventional ferromagnet. In the latter, when the field is reduced from a high value, domain walls are generated to reduce the energy stored in the internal dipolar (demagnetization) field. Furthermore, in an ordinary ferromagnet, the susceptibility does not diverge, but is bounded by the inverse of the demagnetization factor. As has been already pointed out, for $Sr_2Cu_3O_4Cl_2$, the magnetization is much too small to generate domains in this way at the observed high fields. For a conventional ferromagnet, if domain walls are not pinned, the susceptibility reflects the competition between the coupling of the external field to the moment and the coupling of the moments of different domains to each other. As the field is reduced to zero, the total sample moment also goes to zero. Clearly the behavior of domains in $Sr_2Cu_3O_4Cl_2$ is very different. This material gives us a unique possibility to study the detailed behavior of *antiferromagnetic domains*.

One question we must address is how domain walls are generated in the first place. It is helpful in this regard to estimate the domain-wall energy. Because the out-of-plane spin-wave gap is large,[9] we know that the spins remain in the Cu_3O_4 plane. Because of the observed sensitivity to sample shape, we assume that the walls are perpendicular to the Cu_3O_4 plane. Remember that the domain wall is in the Cu_I antiferromagnetic spin system, for which the interaction between the spins is primarily Heisenberg. Therefore, to minimize the energy, the domain wall will extend over many unit cells. The energy of a domain wall per unit cell area is given approximately by

$$U \approx J_I/N + KN, \tag{4}$$

where N is the number of unit cells over which the wall extends and K is the in-plane anisotropy.[12] As usual, this gives a minimum energy for walls of width $N \sim \sqrt{J_I/K}$ and energy per unit area $U \sim \sqrt{J_I K}$. With $J_I \sim 0.1$ eV and $K \sim 10^{-9}$ eV,[7] we find $N \sim 10^4$ unit cells; that is, the width is of order micrometers, and $U \sim 10^{-5}$ eV per unit cell area.

We next present a possible scenario to explain our experimental observations. We start by noting that, while the energy U is very small, a wall that has a macroscopic area is very costly in energy. One way to decrease this cost is to add the entropy associated with the excursions of the wall around its average position, which we denote by S per unit cell area. The *free energy* for creating one wall, $F = U - TS \equiv -\sigma$, may then be negative. The number of walls that are then created is limited by the repulsion between walls, which involves both energy and entropy. This repulsive free energy results from the limitations on the wall excursions, due to the existence of neighboring walls.[13] For a pair of neighboring walls, at an average distance z apart, we denote this (temperature dependent) free energy by $V(z)$ (per unit area of the walls).

We now concentrate on a typical hysteresis curve, e.g., Fig. 4(a). As the field is lowered from high values, M varies continuously in a way that indicates some sort of equilibrium behavior, until one reaches the jump at $-H_{coer}$. In the following discussion, we concentrate on the continuous variation of M in the upper curve; the jump at $-H_{coer}$ is not equilibrium behavior, as is evidenced by the variation in H_{coer} between otherwise identical hysteresis loops, and therefore must be due to additional effects. To explain the upper continuous curve, we note the following experimental facts: (a) As H decreases, domains appear in which the moment is rotated by $\pi/2$. The (single) direction of the moments in these transverse domains is dictated by some residual transverse field. (b) The size and/or the number of these transverse domains increases as H decreases. When H reaches zero, about half of the total moment points in the transverse direction, implying equal volumes of the two types of domains. (See Fig. 5.) The transverse domain size and/or number increases further when H increases in the negative direction, until one reaches $-H_{coer}$. The appearance of transverse domains implies that domain walls become favorable, possibly due to the entropy considerations mentioned above. The other factors imply that we need to consider only one type of domain walls, namely those at which the moments rotate by $\pi/2$.

For simplicity, we now assume parallel planar domain walls, which move and fluctuate only in one direction. We denote this average (linear) size by l. For $T > 100$ K and $H = 0$, the average sizes of the two types of domains are equal to each other. At $H \neq 0$, these sizes are no longer equal, and we denote them by $l_\parallel = l(1+x)$ and $l_\perp = l(1-x)$. At this stage, both l and x may depend on H. However, the magnetizations depend only on x. Assuming that the domains are much larger than the domain walls, $l \gg N$, we then have

$$M = \frac{1+x}{2} M_s, \quad M_t = \frac{1-x}{2} M_s. \tag{5}$$

As H decreases from large positive values to large negative values (ignoring H_{coer}), x varies from 1 to -1, M decreases from M_s to zero and $M_t = M_s - M$. One can thus think of x as an order parameter, which is driven by H.

On the average, when $x \neq 0$, we assume equal numbers of domains of the two kinds, which appear alternately through the system. The mean-field free energy of the domain wall system per unit cell can thus be written as

$$f = [V(l_\parallel) + V(l_\perp) - 2\sigma]/(2l) - HM. \tag{6}$$

In principle, one would now need to minimize f with respect to both l and x, and find both l and x for the equilibrium domain structure. In the absence of a detailed theory for $V(z)$, we prefer to discuss only small values of x, in the vicinity of $H = 0$. In this regime, we neglect the (presumably weak) H dependence of l, expand f in powers of x, and write

$$f = f_0 + \tfrac{1}{2} a x^2 + \tfrac{1}{24} b x^4 - H M_s (1+x)/2, \tag{7}$$

where a and b depend on both T and $l(x=0)$. The latter is to be found by minimizing f_0 with respect to l.

Minimizing now with respect to x, we have

$$ax + \tfrac{1}{6} b x^3 = H M_s/2. \tag{8}$$

Together with $M = M_s(1+x)/2$, this yields curves for M versus H. For $a > 0$ and $b > 0$, these curves look like the upper curve in Fig. 4(a). Furthermore, the theory automatically also yields Figs. 4(b,c).

The susceptibility at the inflection point ($H = 0$) is simply $\chi = M_s^2/(4a)$. The phase transition at 100 K is thus associated with the vanishing of a, when χ diverges and $M(H)$ becomes steep as in Fig. 9. Indeed, we have been able to fit the upper part of the hysteresis curves (for small x) to Eq. (8), with a decreasing towards zero as T decreases towards 100 K. Below 100 K, our theory predicts that $a < 0$ (while still $b > 0$), and thus x approaches a *finite* ''spontaneous'' value as H approaches zero, $x = x_s = \sqrt{-6a/b}$, with slope $\chi = -M_s^2/(8a)$. In this regime, the theory predicts a jump in x at $H = 0$, from x_s to $-x_s$. Our data do not seem to show this jump. Instead, the data below 100 K look similar to those above 100 K, with a smooth variation of M through (roughly) $M_s/2$ at $H = 0$. The slope at $H = 0$ below 100 K also does not agree with the theory (which would predict a

ratio of two between the slopes below and above the transition). At the moment we do not understand this behavior, which must require some modification in the theory. One possibility is that a varies parabolically near the ''transition,'' growing larger and positive below 100 K. Another possibility is that the number of domains changes quickly at low fields near 100 K, due to some unknown mechanism. However, this seems unlikely because nucleation of new domains at H_{coer} is nonequilibrium, implying the existence of a barrier to domain-wall creation. A third possibility involves domain-wall pinning, which might affect the domain-wall dynamics at small fields. We leave all these questions open, for future study.

Since the parameters a and b depend on $V(z)$, the above scenario implies some constraints on the potential. Differentiating Eq. (6), we find that

$$a = l\partial^2 V(z)/\partial z^2|_{z=l(0)}, \quad b = l^3\partial^4 V(z)/\partial z^4|_{z=l(0)}. \quad (9)$$

Minimization with respect to l at $x=0$ implies that $l(0)$ is the solution of

$$V(l) - \sigma = lV'(l). \quad (10)$$

Since both σ and $V(z)$ depend on T, $l(0)$ also depends on T. Thus, a and b depend on T. The above scenario will work if $V(z)$ has an inflection point exactly at $l(0)$, where $a=0$, while $b>0$. Details await a calculation of $V(z)$.

The above scenario assumes equilibrium within a *restricted phase space*, in which there are only two types of domains, with moments along and perpendicular to the external field. Having come from large H, we assume that there exist no domains with negative M. Such domains are created spontaneously at $-H_{coer}$. Once they are created, they immediately grow to cover almost the whole volume, and one moves into the other metastable equilibrium, with only the other two types of domains. (See Figure 5.)

We have considered the possibility that point defects might stabilize domain walls, and have concluded that they cannot. Even if the stabilization energy from point defects were of order J_I it would require many defects within a domain wall width to stabilize the wall. However, in that case, the defect stabilization would overcome the anisotropy cost and the domain-wall width would grow without bound. Another alternative is that domain walls are stabilized by extended defects or dislocations. The simplest example is the crystal surface. Such surfaces could take advantage of the surface spin anisotropy that arises because a Cu_I on the boundary has an unequal number of parallel and perpendicular bonds. There is thus an energy difference of order $(J^{\parallel} - J^{\perp}) \sim 0.04$ meV ~ 150 Oe for a moment parallel or perpendicular to the boundary. This difference could lift the degeneracy between two perpendicular antiferromagnetic arrangements, and may be responsible for the small differences observed in the hysteresis loops for rectangular samples oriented with their long or short sides parallel to the applied magnetic field. If many extended defects exist, this would fix l in the above theory at some quenched value, equal to the average distance between defects. However, one might still continue by introducing the order parameter x and proceeding as above.

In summary, we have presented a complete phenomenology of the magnetization resulting from the motion of antiferromagnetic domain walls in $Sr_2Cu_3O_4Cl_2$. The behavior we have observed, although revealed by the small ferromagnetic moment, results from the behavior of the antiferromagnetic domains and should therefore occur in other antiferromagnetic systems for which there is no equivalent experimental probe of the antiferromagnetic domains. We find that the crystal contains walls between domains with staggered moment parallel and perpendicular to the applied field, probably caused by entropy gains or by extended defects. These walls repel each other, but at 100 K, a phase transition occurs at which the effective compressibility of the domains diverges. To better understand the behavior of this system, one would like to carry out scattering or microscopy experiments to measure the correlations and fluctuations of the walls. However, the very small moments of the domains and the very large length scales involved make this very challenging.

ACKNOWLEDGMENTS

This work has been supported at MIT primarily by the MRSEC Program of the National Science Foundation under Award No. DMR 9808941, and at Tel Aviv and MIT by the U.S.-Israel Binational Science Foundation.

[1] B. Grande and H. Muller-Buschbaum, Z. Naturforsch. B **31B**, 405 (1976).
[2] H. Müller-Buschbaum, Angew. Chem. Int. Ed. Engl. **16**, 674 (1977).
[3] K. Yamada, N. Suzuki, and J. Akimitsu, Physica B **213–214**, 191 (1995).
[4] S. Noro, T. Kouchi, H. Harada, T. Yamadaya, M. Tadokoro, and H. Suzuki, Mater. Sci. Eng., B **25**, 167 (1994).
[5] T. Ito, K. Oka, K. Kojima, G. M. Luke, B. Nachumi, M. Larkin, and Y. J. Uemura, Hyperfine Interact. **104**, 85 (1997).
[6] T. Ito, H. Yamaguchi, and K. Oka, Phys. Rev. B **55**, R684 (1997).
[7] F. C. Chou, A. Aharony, R. J. Birgeneau, O. Entin-Wohlman, M. Greven, A. B. Harris, M. A. Kastner, Y. J. Kim, D. S. Kleinberg, Y. S. Lee, and Q. Zhu, Phys. Rev. Lett. **78**, 535 (1997).
[8] M. A. Kastner, A. Aharony, R. J. Birgeneau, F. C. Chou, O. Entin-Wohlman, M. Greven, A. B. Harris, Y. J. Kim, Y. S. Lee, M. E. Parks, and Q. Zhu, Phys. Rev. B **59**, 14 702 (1999).
[9] Y. J. Kim, A. Aharony, R. J. Birgeneau, F. C. Chou, O. Entin-Wohlman, R. W. Erwin, M. Greven, A. B. Harris, M. A. Kastner, I. Ya. Korenblit, Y. S. Lee, and G. Shirane, Phys. Rev. Lett. **83**, 852 (1999).
[10] E. F. Shender, Zh. Éksp. Teor. Fiz. **83**, 326 (1982) [Sov. Phys.

JETP **56**, 178 (1982)].
[11] T. Yildirim, A. B. Harris, A. Aharony, and O. Entin-Wohlman, Phys. Rev. B **52**, 10 239 (1995).
[12] C. Kittel, *Introduction to Solid State Physics*, 6th ed. (Wiley, New York, 1986), p. 447.
[13] For a review, see P. M. Chaikin and T. C. Lubensky, *Principles of Condensed Matter Physics* (Cambridge University Press, Cambridge, 1995), Sec. 10.6.